Spherical Neutron Polarisation analysis: The Dream 1960 - 2000→

P.J. Brown

Institut Laue Langevin
and
Department of Physics, Loughborough University

F. Tasset symposium 6th March 2009

Contents

1. Introduction: The Blume Maleev Equations
   - Brookhaven 1960
   - The fundamental equations for SNP

Contents

Contents

Contents

Contents

Brookhaven 1960

The history of my interest in polarisation analysis goes back to the early months of my stay at Brookhaven National Lab. as a post-doc 1960-62.

Brookhaven 1960

The history of my interest in polarisation analysis goes back to the early months of my stay at Brookhaven National Lab. as a post-doc 1960-62.

Marty Blume, recently arrived at BNL after spending time in Walter Marshal's group at Harwell was persuaded by Bob Nathans to give some informal lectures on Neutron scattering to his research group.

Brookhaven 1960

The history of my interest in polarisation analysis goes back to the early months of my stay at Brookhaven National Lab. as a post-doc 1960-62.

Marty Blume, recently arrived at BNL after spending time in Walter Marshal's group at Harwell was persuaded by Bob Nathans to give some informal lectures on Neutron scattering to his research group.

Here is an extract from the notes that I made on the polarisation dependence of the scattering cross-section.

The polarisation of the scattered beam:

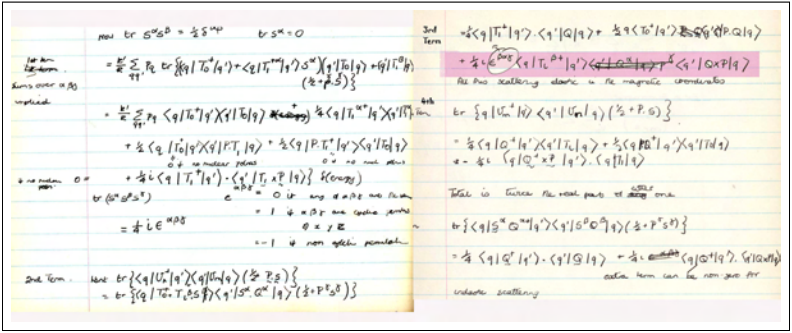

The polarisation of the scattered beam:

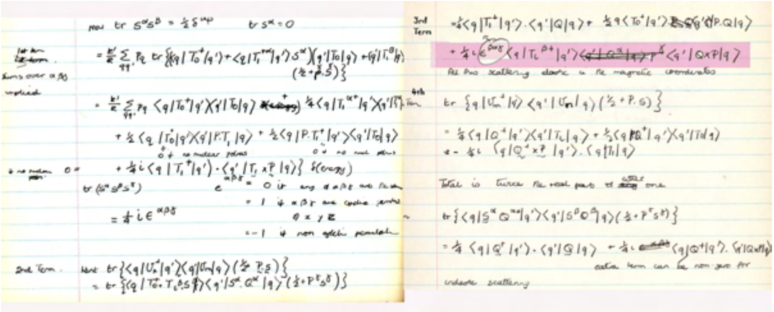

This same equation, tidied up, appears again a little later in the *Blume Maleev equations.*

Blume 1973

Equation 19 from M Blume, *Phys. Rev.* **130** 1670 (1963)

Blume 1973

Equation 19 from M Blume, *Phys. Rev.* **130** 1670 (1963)

$$\begin{aligned}\tfrac12 \mathbf{P}_f \frac{d\sigma}{d\Omega'} = {} & \tfrac12 \mathbf{P}\Big|\sum_n e^{i\mathbf{K}\cdot\mathbf{n}}\Big|^2 |F_N(\mathbf{K})|^2 - \tfrac12 \mathbf{P} N \sum_j \left(\tfrac13\langle\{a_j^2\}\rangle - \tfrac13\langle\{a_j\}^2\rangle + \langle\{a_j\}\rangle^2\right) + \frac12\left(\frac{\gamma e^2}{mc^2}\right)\sum_{nj,n'j'} \exp[i\mathbf{K}\cdot(\mathbf{R}_{nj}-\mathbf{R}_{n'j'})] \\ & \times\Big(\langle\{a_{j'}\}\rangle S_{nj} f_{nj}(\mathbf{K})\mathbf{q}_{nj} + \langle\{a_j\}\rangle S_{n'j'} f_{n'j'}^*(\mathbf{K})\mathbf{q}_{n'j'} - i\langle\{a_{j'}\}\rangle S_{nj} f_{nj}(\mathbf{K})(\mathbf{P}\times\mathbf{q}_{nj}) \\ & + i\langle\{a_j\}\rangle S_{n'j'} f_{n'j'}^*(\mathbf{K})(\mathbf{P}\times\mathbf{q}_{n'j'})\Big) + \frac12\left(\frac{\gamma e^2}{mc^2}\right)^2 \sum_{nj,n'j'} \exp[i\mathbf{K}\cdot(\mathbf{R}_{nj}-\mathbf{R}_{n'j'})] S_{n'j'} S_{nj} f_{n'j'}^*(\mathbf{K}) f_{nj}(\mathbf{K}) \\ & \times\Big(-i(\mathbf{q}_{n'j'}\times\mathbf{q}_{nj}) + \mathbf{q}_{n'j'}(\mathbf{P}\cdot\mathbf{q}_{nj}) + (\mathbf{P}\cdot\mathbf{q}_{n'j'})\mathbf{q}_{nj} - \mathbf{P}(\mathbf{q}_{n'j'}\cdot\mathbf{q}_{nj})\Big).\end{aligned}$$

At almost the same time, essentially the same equations were elaborated by Serge Maleev.

S.V. Maleev, V.G. Bar'yaktar and R.A.Suris, *Sov. Phys. - Solid State* **4** 2533 (1963)

Equation 19 from M Blume,*Phys. Rev.* **130** 1670 (1963)

$$\tfrac{1}{2}\mathbf{P}_f \frac{d\sigma}{d\Omega'} = \tfrac{1}{2}\mathbf{P}\left|\sum_{\mathbf{n}} e^{i\mathbf{K}\cdot\mathbf{n}}\right|^2 |F_N(\mathbf{K})|^2 - \tfrac{1}{2}\mathbf{P}N\sum_j \left(\tfrac{1}{3}\langle\{a_j^2\}\rangle - \tfrac{4}{3}\langle\{a_j\}^2\rangle + \langle\{a_j\}\rangle^2\right) + \frac{1}{2}\left(\frac{\gamma e^2}{mc^2}\right)\sum_{\mathbf{n}j,\mathbf{n}'j'} \exp[i\mathbf{K}\cdot(\mathbf{R}_{\mathbf{n}j}-\mathbf{R}_{\mathbf{n}'j'})]$$
$$\times\Big(\langle\{a_{j'}\}\rangle S_{\mathbf{n}j} f_{\mathbf{n}j}(\mathbf{K})\mathbf{q}_{\mathbf{n}j} + \langle\{a_j\}\rangle S_{\mathbf{n}'j'} f_{\mathbf{n}'j'}^*(\mathbf{K})\mathbf{q}_{\mathbf{n}'j'} - i\langle\{a_{j'}\}\rangle S_{\mathbf{n}j} f_{\mathbf{n}j}(\mathbf{K})(\mathbf{P}\times\mathbf{q}_{\mathbf{n}j})$$
$$+ i\langle\{a_j\}\rangle S_{\mathbf{n}'j'} f_{\mathbf{n}'j'}^*(\mathbf{K})(\mathbf{P}\times\mathbf{q}_{\mathbf{n}'j'})\Big) + \frac{1}{2}\left(\frac{\gamma e^2}{mc^2}\right)^2 \sum_{\mathbf{n}j,\mathbf{n}'j'} \exp[i\mathbf{K}\cdot(\mathbf{R}_{\mathbf{n}j}-\mathbf{R}_{\mathbf{n}'j'})] S_{\mathbf{n}'j'} S_{\mathbf{n}j} f_{\mathbf{n}'j'}^*(\mathbf{K}) f_{\mathbf{n}j}(\mathbf{K})$$
$$\times\Big(-i(\mathbf{q}_{\mathbf{n}'j'}\times\mathbf{q}_{\mathbf{n}j}) + \mathbf{q}_{\mathbf{n}'j'}(\mathbf{P}\cdot\mathbf{q}_{\mathbf{n}j}) + (\mathbf{P}\cdot\mathbf{q}_{\mathbf{n}'j'})\mathbf{q}_{\mathbf{n}j} - \mathbf{P}(\mathbf{q}_{\mathbf{n}'j'}\cdot\mathbf{q}_{\mathbf{n}j})\Big).$$

At almost the same time, essentially the same equations were elaborated by Serge Maleev.

S.V. Maleev,V.G. Bar'yaktar and R.A.Suris,*Sov. Phys. - Solid State* **4** 2533 (1963)

The *Dream for Spherical neutron polarimetry* is to be able to measure all the terms in these equations precisely.

The Blume-Maleev Equations written in terms of Structure Factors

The scattered polarisation $\mathbf{P}'$ and scattered intensity I for incident polarisation $\mathbf{P}$ can be written as:

The Blume-Maleev Equations written in terms of Structure Factors

The scattered polarisation $\mathbf{P}'$ and scattered intensity I for incident polarisation $\mathbf{P}$ can be written as:

$$\mathbf{P}'I \quad = \quad \mathbf{P}(|N(\mathbf{k})|^2 - \mathbf{M}_\perp(\mathbf{k}) \cdot \mathbf{M}^*_\perp(\mathbf{k})) \quad \text{part parallel to } \mathbf{P}$$

The scattered polarisation $\mathbf{P}'$ and scattered intensity I for incident polarisation $\mathbf{P}$ can be written as:

$$
\begin{aligned}
\mathbf{P}'I \quad = \quad & \mathbf{P}(|N(\mathbf{k})|^2 - \mathbf{M}_\perp(\mathbf{k}) \cdot \mathbf{M}^*_\perp(\mathbf{k})) \quad \text{part parallel to } \mathbf{P} \\
& + 2\Re[\mathbf{M}_\perp(\mathbf{P} \cdot \mathbf{M}^*_\perp(\mathbf{k}))] \\
& + 2\Re[\mathbf{M}_\perp(\mathbf{k})N^*(\mathbf{k})] \quad \text{part parallel to } \mathbf{M}_\perp
\end{aligned}
$$

The Blume-Maleev Equations written in terms of Structure Factors

The scattered polarisation $\mathbf{P}'$ and scattered intensity I for incident polarisation $\mathbf{P}$ can be written as:

$$
\begin{aligned}
\mathbf{P}'I \quad = \quad & \mathbf{P}(|N(\mathbf{k})|^2 - \mathbf{M}_\perp(\mathbf{k})\cdot\mathbf{M}^*_\perp(\mathbf{k})) \quad \text{part parallel to } \mathbf{P} \\
& + 2\Re[\mathbf{M}_\perp(\mathbf{P}\cdot\mathbf{M}^*_\perp(\mathbf{k}))] \\
& + 2\Re[\mathbf{M}_\perp(\mathbf{k})N^*(\mathbf{k})] \quad \text{part parallel to } \mathbf{M}_\perp \\
& + \mathbf{P}\times 2\Im(\mathbf{M}_\perp N^*(\mathbf{k})) \quad \text{part perpendicular to } \mathbf{P} \text{ and } \mathbf{M}_\perp \\
& - \Im\mathbf{M}_\perp(\mathbf{k})\times\mathbf{M}^*_\perp(\mathbf{k})) \quad \text{part parallel to } \mathbf{k}
\end{aligned}
$$

The Blume-Maleev Equations written in terms of Structure Factors

The scattered polarisation $\mathbf{P}'$ and scattered intensity I for incident polarisation $\mathbf{P}$ can be written as:

$$\begin{aligned}
\mathbf{P}'I &= \mathbf{P}(|N(\mathbf{k})|^2 - \mathbf{M}_\perp(\mathbf{k}) \cdot \mathbf{M}^*_\perp(\mathbf{k})) \quad \text{part parallel to } \mathbf{P} \\
&+ 2\Re[\mathbf{M}_\perp(\mathbf{P} \cdot \mathbf{M}^*_\perp(\mathbf{k}))] \\
&+ 2\Re[\mathbf{M}_\perp(\mathbf{k})N^*(\mathbf{k})] \quad \text{part parallel to } \mathbf{M}_\perp \\
&+ \mathbf{P} \times 2\Im(\mathbf{M}_\perp N^*(\mathbf{k})) \quad \text{part perpendicular to } \mathbf{P} \text{ and } \mathbf{M}_\perp \\
&- \Im\mathbf{M}_\perp(\mathbf{k}) \times \mathbf{M}^*_\perp(\mathbf{k})) \quad \text{part parallel to } \mathbf{k} \\
I &= |N(\mathbf{k})|^2 + \mathbf{M}_\perp(\mathbf{k}) \cdot \mathbf{M}^*_\perp(\mathbf{k}) \quad \text{polarisation independent part}
\end{aligned}$$

The scattered polarisation $\mathbf{P}'$ and scattered intensity I for incident polarisation $\mathbf{P}$ can be written as:

$$\begin{aligned}
\mathbf{P}'I \;=\; & \mathbf{P}(|N(\mathbf{k})|^2 - \mathbf{M}_\perp(\mathbf{k})\cdot\mathbf{M}^*_\perp(\mathbf{k})) \quad \text{part parallel to } \mathbf{P} \\
& + 2\Re[\mathbf{M}_\perp(\mathbf{P}\cdot\mathbf{M}^*_\perp(\mathbf{k}))] \\
& + 2\Re[\mathbf{M}_\perp(\mathbf{k})N^*(\mathbf{k})] \quad \text{part parallel to } \mathbf{M}_\perp \\
& + \mathbf{P}\times 2\Im(\mathbf{M}_\perp N^*(\mathbf{k})) \quad \text{part perpendicular to } \mathbf{P} \text{ and } \mathbf{M}_\perp \\
& - \Im\mathbf{M}_\perp(\mathbf{k})\times\mathbf{M}^*_\perp(\mathbf{k})) \quad \text{part parallel to } \mathbf{k}
\end{aligned}$$

$$\begin{aligned}
I \;=\; & |N(\mathbf{k})|^2 + \mathbf{M}_\perp(\mathbf{k})\cdot\mathbf{M}^*_\perp(\mathbf{k}) \quad \text{polarisation independent part} \\
& + 2\Re(\mathbf{P}\cdot\mathbf{M}_\perp(\mathbf{k})N^*(\mathbf{k})) \\
& + \mathbf{P}\cdot\Im(\mathbf{M}_\perp(\mathbf{k})\times\mathbf{M}^*_\perp(\mathbf{k})) \quad \text{polarisation dependent parts}
\end{aligned}$$

Cr_2O_3 Alperin 1973

The first experiment to verify the polarisation rotation predicted by the Blume-Maleev equations was made by Harvey Alperin and reported at the International Magnetism Conference in Moscow in 1973.

Cr_2O_3 Alperin 1973

The first experiment to verify the polarisation rotation predicted by the Blume-Maleev equations was made by Harvey Alperin and reported at the International Magnetism Conference in Moscow in 1973.

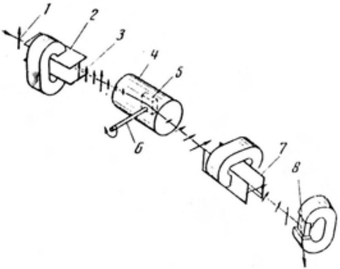

Figure 1. Experimental arrangement to analyze polarization in a direction perpendicular to incident direction.

1-polarized neutron, 2,7--magnetic guides,

3-magnetic field (direction and magnitude indicated).

4-soft iron magnetic shield, 5-Cr_2O_3 crystal,

6-shaft for rotating crystal about [110], 8-$Co_{.92}$ $Fe_{.08}$ analyzing crystal.

Cr_2O_3 Alperin Results

A Cr_2O_3 crystal which has an anti-centrosymmetric magnetic structure and a Néel temperature ≈ 310 K was mounted so that it could be rotated about a 102 scattering vector

Cr_2O_3 Alperin Results

A Cr_2O_3 crystal which has an anti-centrosymmetric magnetic structure and a Néel temperature ≈ 310 K was mounted so that it could be rotated about a 102 scattering vector

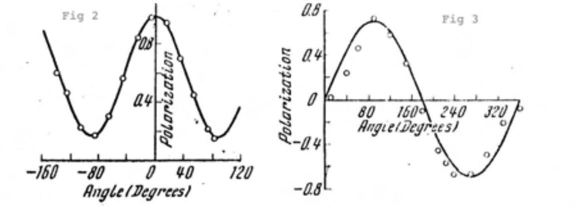

Figure 2. Polarization analysis in direction parallel to incident polarization Circles--experimental points, smooth curve--theoretical prediction (see text).

Figure 3. Polarization analysis in direction perpendicular to incident polarization. Circles--experimental points, smooth curve--theoretical prediction

Cr_2O_3 Alperin Results

A Cr_2O_3 crystal which has an anti-centrosymmetric magnetic structure and a Néel temperature ≈ 310 K was mounted so that it could be rotated about a 102 scattering vector

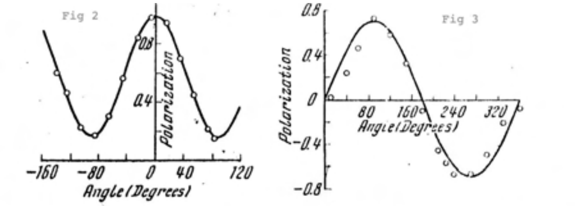

Figure 2. Polarization analysis in direction parallel to incident polarization Circles--experimental points, smooth curve--theoretical prediction (see text).

Figure 3. Polarization analysis in direction perpendicular to incident polarization. Circles--experimental points, smooth curve--theoretical prediction

- When the direction of analysis is parallel to the incident polarisation full polarisation is observed at $\phi = 0$, (trigonal axis parallel to P_{in}.

Cr_2O_3 Alperin Results

A Cr_2O_3 crystal which has an anti-centrosymmetric magnetic structure and a Néel temperature ≈ 310 K was mounted so that it could be rotated about a 102 scattering vector

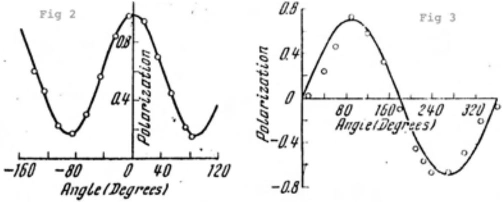

Figure 2. Polarization analysis in direction parallel to incident polarization Circles--experimental points, smooth curve--theoretical prediction (see text).

Figure 3. Polarization analysis in direction perpendicular to incident polarization. Circles--experimental points, smooth curve--theoretical prediction

- When the direction of analysis is parallel to the incident polarisation full polarisation is observed at $\phi = 0$, (trigonal axis parallel to P_{in}.
- When the direction of analysis is perpendicular to the incident polarisation the maximum polarisation is 0.6 with $\phi = 90°$, (trigonal axis in plane perpendical to P_{in}.

Cr_2O_3 Alperin's Conclusions

Conclusions

Measurements on Cr_2O_3 yield observations of all the important terms in the general expression for the final polarization of polarized neutrons scattered from a magnetic crystal. The first and fourth terms of equation (2) previously measured by Nathans et. al.[4] are verified here and excellent agreement is obtained as shown in Figure 3. The $(\hat{P}_i \times \hat{q})$-term derived by Blume is measured here for the first time. The deviations from theory (Figure 3) are due most likely to stray fields inside the magnetic shield which cause $\vec{P}_i$ and $\vec{P}_a$ to deviate from their assumed directions.

For crystals of general symmetry, measurements of the final polarization in two perpendicular directions as well as the cross section are necessary in order to completely determine the magnetic and nuclear structure factors and their phases. For an anti-centrosymmetric magnetic crystal one cannot obtain information about antiferromagnetic domains by measuring the cross section or by only analyzing the polarization in the direction $\hat{P}_i$.

Vector character of magnetisation distributions

- Measurement of the scattered polarisation provides more direct access to the vector properties of the magnetisation distribution than do intensity measurements.

Vector character of magnetisation distributions

- Measurement of the scattered polarisation provides more direct access to the vector properties of the magnetisation distribution than do intensity measurements.
- The magnetisation distribution will be non-collinear if the spin-orbit coupling is important

Vector character of magnetisation distributions

- Measurement of the scattered polarisation provides more direct access to the vector properties of the magnetisation distribution than do intensity measurements.
- The magnetisation distribution will be non-collinear if the spin-orbit coupling is important
- Can polarisation analysis experiments have sufficient precision to determine such non-collinearity?

Vector character of magnetisation distributions

Non-collinear *spin density* due to spin orbit coupling λ between 3d electrons (x-z plane)

Vector character of magnetisation distributions

Non-collinear *spin density* due to spin orbit coupling λ between 3d electrons (x-z plane)

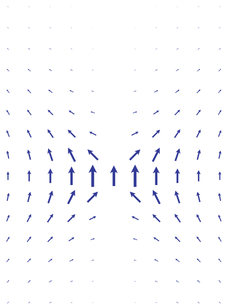

$m = 2, s = -\frac{1}{2}$ with $m = 1, s = \frac{1}{2}$

$$\rho_z \propto (x^2 - y^2)^2 - \lambda^2 z^2 (x^2 + y^2)$$

$$\rho_x \propto \lambda xz(x^2 - y^2)$$

Non-collinear *spin density* due to spin orbit coupling λ between 3d electrons (x-z plane)

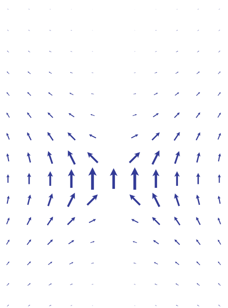

$$m = 2, s = -\tfrac{1}{2} \text{ with } m = 1, s = \tfrac{1}{2}$$
$$\rho_z \propto (x^2 - y^2)^2 - \lambda^2 z^2 (x^2 + y^2)$$
$$\rho_x \propto \lambda xz(x^2 - y^2)$$

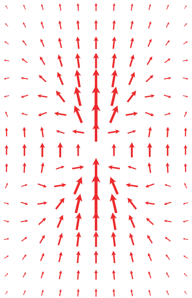

$$m = 0, s = \tfrac{1}{2} \text{ with } m = 1, s = -\tfrac{1}{2}$$
$$\rho_z \propto (3x^2 - r^2)^2 - \lambda^2 z^2 (x^2 + y^2)$$
$$\rho_x \propto \lambda xz(3z^2 - r^2)$$

Non-collinear 3d *Orbital moment density* (x-z plane)

Vector character of magnetisation distributions

Non-collinear 3d *Orbital moment density* (x-z plane)

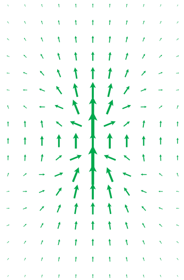

The orbital moment distribution due to an imbalance δ in the occupancy of 3d states with $m = \pm 2$

$$\rho_z \propto 4\delta(x^2 - y^2)^2$$

$$\rho_x \propto 2\delta z(x^3 - xy^2)$$

Spin-Orbit coupling in $FeCO_3$

An attempt to demonstrate non-collinearity due to spin-orbit coupling in $FeCO_3$ using polarisation analysis (1975)

P J Brown and J B Forsyth, *J. Phys C: Solid State Phys* **10** 3157 (1977)

An attempt to demonstrate non-collinearity due to spin-orbit coupling in $FeCO_3$ using polarisation analysis (1975)

P J Brown and J B Forsyth, *J. Phys C: Solid State Phys* **10** 3157 (1977)

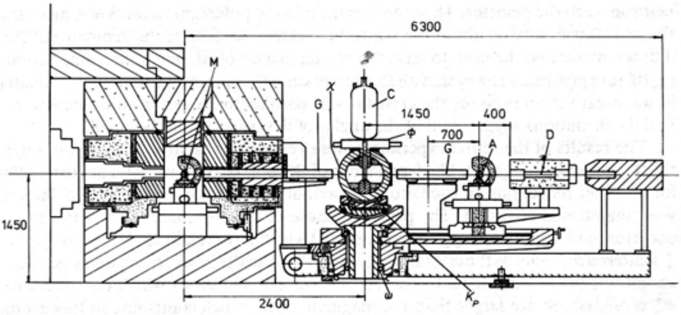

Experiment carried out using D5 in polarisation analysis mode

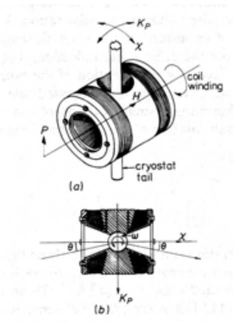

A special coil around the cryostat tail rotates the polarisation into a direction in the scattering plane perpendicular to the scattering vector

Spin-Orbit coupling in $FeCO_3$

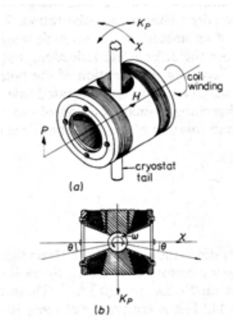

A special coil around the cryostat tail rotates the polarisation into a direction in the scattering plane perpendicular to the scattering vector

- The sample was rotated about the scattering vector using the χ circle to find the direction of maximum scattered polarisation.

Spin-Orbit coupling in $FeCO_3$

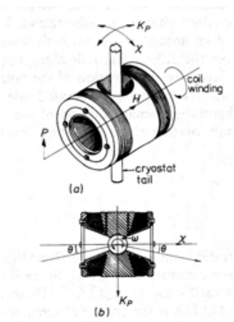

A special coil around the cryostat tail rotates the polarisation into a direction in the scattering plane perpendicular to the scattering vector

- The sample was rotated about the scattering vector using the χ circle to find the direction of maximum scattered polarisation.
- No non-collinearity was found ($\chi_{\text{max}} = 0$), probably due to 180° domains.

Spin-Orbit coupling in $FeCO_3$

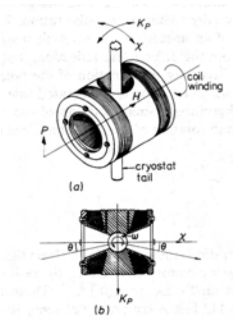

A special coil around the cryostat tail rotates the polarisation into a direction in the scattering plane perpendicular to the scattering vector

- The sample was rotated about the scattering vector using the χ circle to find the direction of maximum scattered polarisation.
- No non-collinearity was found ($\chi_{\text{max}} = 0$), probably due to 180° domains.
- Precision limited by variation of multiple scattering as the sample was rotated.

Cryopad I

- The variation of multiple scattering can be avoided if the polarisation, rather than the crystal is rotated to find the scattered polarisation direction.

Cryopad I

- The variation of multiple scattering can be avoided if the polarisation, rather than the crystal is rotated to find the scattered polarisation direction.
- Superconducting shields can be used to separate different precession regimes.

Cryopad I

- The variation of multiple scattering can be avoided if the polarisation, rather than the crystal is rotated to find the scattered polarisation direction.
- Superconducting shields can be used to separate different precession regimes.
- An existing, but disused cryostat was modified by Francis and Serge Pujol to make CRYoPAD I.

Cryopad I

- The variation of multiple scattering can be avoided if the polarisation, rather than the crystal is rotated to find the scattered polarisation direction.
- Superconducting shields can be used to separate different precession regimes.
- An existing, but disused cryostat was modified by Francis and Serge Pujol to make CRYoPAD I.

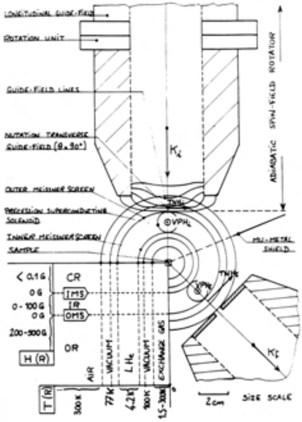

F. Tasset, *Proceedings ICNS 88 Grenoble* (1988)

The Cr_2O_3 saga

The first real test of CRYOPAD I was to obtain a result equivalent to Alperin's experiment on Cr_2O_3

The first real test of CRYOPAD I was to obtain a result equivalent to Alperin's experiment on Cr_2O_3

Pages from the notebook

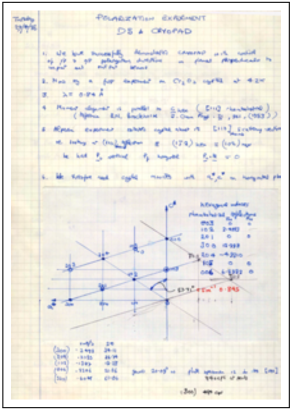

The Cr_2O_3 saga

The first real test of CRYOPAD I was to obtain a result equivalent to Alperin's experiment on Cr_2O_3

Pages from the notebook

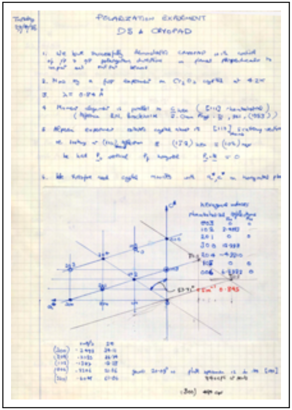

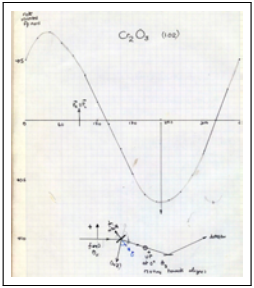

The Cr_2O_3 saga

The first real test of CRYOPAD I was to obtain a result equivalent to Alperin's experiment on Cr_2O_3

Pages from the notebook

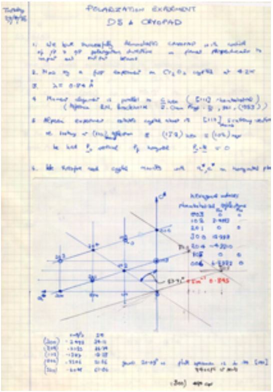

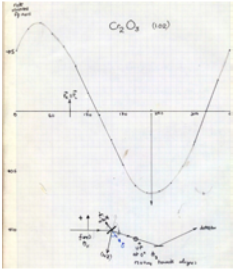

$\mathbf{P}' \parallel \mathbf{P}$ for $\theta_2 = 90^\circ$ $\mathbf{P}' = -0.45 = P_0 P_{eff}; P_0 = \frac{1-\gamma^2}{1+\gamma^2}$ -> $\gamma = 1.9$

$\mathbf{P}' = 0$ for $\theta_2 = 135$ and 320° giving $\theta_r = 137.5^\circ$

$\tan\theta_r = \frac{2\gamma\eta}{1+\gamma^2}$ where $\eta = 0.65$ is the domain fraction $\frac{v_1 - v_2}{v_1 + v_2}$ and v_1, v_2 are the volumes of the two 180° domains.

The Néel temperature from SNP measurements

The rotation effect should go to zero at the Néel temperature

The Néel temperature from SNP measurements

The rotation effect should go to zero at the Néel temperature

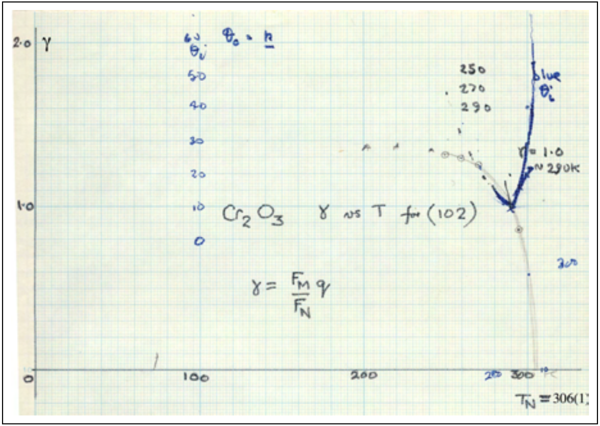

The Néel temperature from SNP measurements

The rotation effect should go to zero at the Néel temperature

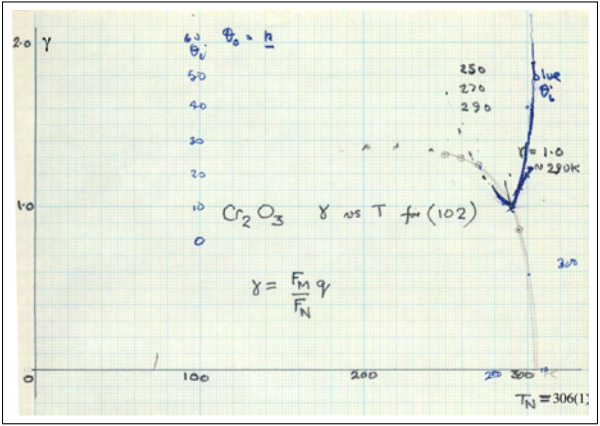

With $\mathbf{P}'$ parallel to the scattering vector $\mathbf{k}$ $\theta_1 = 0$, $\mathbf{P} \perp \mathbf{k}$ when $\gamma = 1$

The polarisation tensor

When using CRYOPAD it has been found convenient to define the polarisation directions using a set of *Polarisation axes* rather than with the θ and ϕ angles of the CRYOPAD.

The polarisation tensor

When using CRYOPAD it has been found convenient to define the polarisation directions using a set of *Polarisation axes* rather than with the θ and ϕ angles of the CRYOPAD.

The *Polarisation axes* are defined with:

- x parallel to the scattering vector $\mathbf{k}$.
- z perpendicular to the scattering plane (vertical)
- y completing the right handed cartesian set

The polarisation tensor

When using CRYOPAD it has been found convenient to define the polarisation directions using a set of *Polarisation axes* rather than with the θ and ϕ angles of the CRYOPAD.

The *Polarisation axes* are defined with:

- x parallel to the scattering vector $\mathbf{k}$.
- z perpendicular to the scattering plane (vertical)
- y completing the right handed cartesian set

With this choice of axes there are no components of the magnetic interaction vector $\mathbf{M}_{\perp}(\mathbf{k})$ parallel to x.

The polarisation tensor

When using CRYOPAD it has been found convenient to define the polarisation directions using a set of *Polarisation axes* rather than with the θ and ϕ angles of the CRYOPAD.

The *Polarisation axes* are defined with:

- x parallel to the scattering vector $\mathbf{k}$.
- z perpendicular to the scattering plane (vertical)
- y completing the right handed cartesian set

With this choice of axes there are no components of the magnetic interaction vector $\mathbf{M}_\perp(\mathbf{k})$ parallel to x.

The Blume Maleev equations can be written in tensor form

$$\mathbf{P}' = \mathsf{\mathbf{P}}\mathbf{P} + \mathbf{P}'' \quad \text{or in components} \quad P'_i = \mathsf{P}_{ij}P_j + P''_i$$

$\mathbf{P}''$ is the polarisation created in the scattering process.

The polarisation tensor in polarisation coordinates

The polarisation tensor on polarisation axes becomes:

$$\mathbf{P} = \begin{pmatrix} (N^2 - M^2)/I_x & J_{nz}/I_x & J_{ny}/I_x \\ -J_{nz}/I_y & (N^2 - M^2 + R_{yy})/I_y & R_{yz}/I_y \\ -J_{ny}/I_z & R_{zy}/I_z & (N^2 - M^2 + R_{zz})/I_z \end{pmatrix}$$

And the polarisation created is

$$\mathbf{P}'' = \begin{pmatrix} -J_{yz}/I \\ R_{ny}/I \\ R_{nz}/I \end{pmatrix} \qquad \begin{aligned} I_x &= M^2 + N^2 + P_x J_{yz} \\ I_y &= M^2 + N^2 + P_y R_{ny} \\ I_z &= M^2 + N^2 + P_z R_{nz} \\ I &= M^2 + N^2 + P_x J_{yz} + P_y R_{ny} + P_z R_{nz} \end{aligned}$$

$$\begin{aligned} N^2 &= N(\mathbf{k})N^*(\mathbf{k}) \\ R_{ij} &= 2\Re(M_{\perp i}(\mathbf{k}) M_{\perp j}{}^*(\mathbf{k})) \\ J_{ij} &= 2\Im(M_{\perp i}(\mathbf{k}) M_{\perp j}{}^*(\mathbf{k})) \end{aligned} \qquad \begin{aligned} M^2 &= \mathbf{M}_\perp(\mathbf{k}) \cdot \mathbf{M}_\perp(\mathbf{k}) \\ R_{ni} &= 2\Re(N(\mathbf{k}) M_{\perp i}{}^*(\mathbf{k})) \\ J_{ni} &= 2\Im(N(\mathbf{k}) M_{\perp i}{}^*(\mathbf{k})) \end{aligned}$$

The polarisation tensor in polarisation coordinates

The polarisation tensor on polarisation axes becomes:

$$\mathbf{P} = \begin{pmatrix} (N^2 - M^2)/I_x & J_{nz}/I_x & J_{ny}/I_x \\ -J_{nz}/I_y & (N^2 - M^2 + R_{yy})/I_y & R_{yz}/I_y \\ -J_{ny}/I_z & R_{zy}/I_z & (N^2 - M^2 + R_{zz})/I_z \end{pmatrix}$$

And the polarisation created is

$$\mathbf{P}'' = \begin{pmatrix} -J_{yz}/I \\ R_{ny}/I \\ R_{nz}/I \end{pmatrix} \qquad \begin{aligned} I_x &= M^2 + N^2 + P_x J_{yz} \\ I_y &= M^2 + N^2 + P_y R_{ny} \\ I_z &= M^2 + N^2 + P_z R_{nz} \\ I &= M^2 + N^2 + P_x J_{yz} + P_y R_{ny} + P_z R_{nz} \end{aligned}$$

$$\begin{aligned} N^2 &= N(\mathbf{k})N^*(\mathbf{k}) \\ R_{ij} &= 2\Re(M_{\perp i}(\mathbf{k})M_{\perp j}{}^*(\mathbf{k})) \\ J_{ij} &= 2\Im(M_{\perp i}(\mathbf{k})M_{\perp j}{}^*(\mathbf{k})) \end{aligned} \qquad \begin{aligned} M^2 &= \mathbf{M}_\perp(\mathbf{k}) \cdot \mathbf{M}_\perp(\mathbf{k}) \\ R_{ni} &= 2\Re(N(\mathbf{k})M_{\perp i}{}^*(\mathbf{k})) \\ J_{ni} &= 2\Im(N(\mathbf{k})M_{\perp i}{}^*(\mathbf{k})) \end{aligned}$$

Note that when written in this simplified way **P** isn't strictly a tensor because the denominators depend on the incident polarisation.

Polarisation Matrices: The experimental data

The usual experimental strategy is to measure the scattered polarisation $\mathbf{P}'$ with the incident polarisation $\mathbf{P}$ parallel to polarisation x, y, z in turn.
This determines the polarisation matrix.

Polarisation Matrices: The experimental data

The usual experimental strategy is to measure the scattered polarisation $\mathbf{P}'$ with the incident polarisation $\mathbf{P}$ parallel to polarisation x, y, z in turn.
This determines the polarisation matrix.

The *polarisation matrix* P_{ij} is the experimentally measurable quantity related to the polarisation tensor.
The matrix element P_{ij} gives the ith component of scattered polarisation when the incident polarisation is in the jth direction.

$$P_{ij} = \left\langle \frac{\mathsf{P}_{ij} P_j + P''_i}{P_j} \right\rangle_{\text{domains}}$$

Rotation of the polarisation

Off-diagonal terms in the polarisation matrix correspond to rotation of the polarisation direction.

They are of two kinds.

Rotation of the polarisation

Off-diagonal terms in the polarisation matrix correspond to rotation of the polarisation direction.
They are of two kinds.

1. P_{yz} and P_{zy} which depend upon $R_{yz} = 2\Re(M_{\perp y}(\mathbf{k})M_{\perp z}{}^{*}(\mathbf{k}))$

Rotation of the polarisation

Off-diagonal terms in the polarisation matrix correspond to rotation of the polarisation direction.

They are of two kinds.

1. P_{yz} and P_{zy} which depend upon $R_{yz} = 2\Re(M_{\perp y}(\mathbf{k})M_{\perp z}{}^{*}(\mathbf{k}))$
   They can be reduced to zero by choosing either the y or z axis parallel to $\mathbf{M}_{\perp}$.

Rotation of the polarisation

Off-diagonal terms in the polarisation matrix correspond to rotation of the polarisation direction.

They are of two kinds.

1. P_{yz} and P_{zy} which depend upon $R_{yz} = 2\Re(M_{\perp y}(\mathbf{k})M_{\perp z}{}^{*}(\mathbf{k}))$ They can be reduced to zero by choosing either the y or z axis parallel to $\mathbf{M}_{\perp}$.
2. Elements P_{xy}, P_{xz}, P_{yx} and P_{zx} which represent rotations towards, or away from, the scattering vector.

Rotation of the polarisation

Off-diagonal terms in the polarisation matrix correspond to rotation of the polarisation direction.

They are of two kinds.

1. P_{yz} and P_{zy} which depend upon $R_{yz} = 2\Re(M_{\perp y}(\mathbf{k})M_{\perp z}{}^*(\mathbf{k}))$
   They can be reduced to zero by choosing either the y or z axis parallel to $\mathbf{M}_\perp$.
2. Elements P_{xy}, P_{xz}, P_{yx} and P_{zx} which represent rotations towards, or away from, the scattering vector.
   They depend on $\Im(\mathbf{M}_\perp N^*)$ and are always present when nuclear and magnetic scattering occur together with a phase difference which is neither 0 or π.

Polarisation rotation and the magneto-electric effect

- It finally dawned on us that the symmetry requirements for a structure which will rotate the polarisation towards the scattering vector are almost the same as those required for a non-zero magneto-electric effect.

Polarisation rotation and the magneto-electric effect

- It finally dawned on us that the symmetry requirements for a structure which will rotate the polarisation towards the scattering vector are almost the same as those required for a non-zero magneto-electric effect.
- The sense of the rotation differs for the two 180° domains as do the signs of the magneto-electric coefficients.

Polarisation rotation and the magneto-electric effect

- It finally dawned on us that the symmetry requirements for a structure which will rotate the polarisation towards the scattering vector are almost the same as those required for a non-zero magneto-electric effect.
- The sense of the rotation differs for the two 180° domains as do the signs of the magneto-electric coefficients.
- The domain ratio η can be measured using SNP which allows the intrinsic magneto-electric coefficients to be determined.

Polarisation rotation and the magneto-electric effect

- It finally dawned on us that the symmetry requirements for a structure which will rotate the polarisation towards the scattering vector are almost the same as those required for a non-zero magneto-electric effect.
- The sense of the rotation differs for the two 180° domains as do the signs of the magneto-electric coefficients.
- The domain ratio η can be measured using SNP which allows the intrinsic magneto-electric coefficients to be determined.

If the moments are parallel to polarisation z

$$\boldsymbol{P} = \begin{pmatrix} \beta & \eta\xi & 0 \\ -\eta\xi & \beta & 0 \\ 0 & 0 & 1 \end{pmatrix} \quad \text{with} \quad \begin{aligned} \beta &= (1-\gamma^2)/(1+\gamma^2) \\ \xi &= 2q_z\gamma/(1+\gamma^2) \\ \gamma &= \mathbf{M}_\perp(\mathbf{k})/N(\mathbf{k}) \end{aligned}$$

q_z is $+1$ if $\mathbf{M}(\mathbf{k})$ is parallel to $\mathbf{z}$ and -1 if it is antiparallel.

180° domain populations: CRYOPAD I on IN20

- Measurement of the polarisation matrix allows both η and γ to be determined.

180° domain populations: CRYOPAD I on IN20

- Measurement of the polarisation matrix allows both η and γ to be determined.
- The effects of electric and magnetic fields on the domain population can be studied.

180° domain populations: CRYOPAD I on IN20

- Measurement of the polarisation matrix allows both η and γ to be determined.
- The effects of electric and magnetic fields on the domain population can be studied.
- When $\eta \neq 0$ the absolute directions of rotation of the neutron spins determine the magnetic configuration of the more populous domain.

180° domain populations: CRYOPAD I on IN20

- Measurement of the polarisation matrix allows both η and γ to be determined.
- The effects of electric and magnetic fields on the domain population can be studied.
- When $\eta \neq 0$ the absolute directions of rotation of the neutron spins determine the magnetic configuration of the more populous domain.
- For these experiments the sample must be removed from the cryopad, warmed above its Néel temperature, then cooled through the Néel transition under the chosen conditions of electric and magnetic field.

180° domain populations: CRYOPAD I on IN20

- Measurement of the polarisation matrix allows both η and γ to be determined.
- The effects of electric and magnetic fields on the domain population can be studied.
- When $\eta \neq 0$ the absolute directions of rotation of the neutron spins determine the magnetic configuration of the more populous domain.
- For these experiments the sample must be removed from the cryopad, warmed above its Néel temperature, then cooled through the Néel transition under the chosen conditions of electric and magnetic field.
- For Cr_2O_3 the symmetry of the magnetic structure suggests the fields should be applied parallel to the trigonal axis.

180° domain populations: CRYOPAD I on IN20

- Measurement of the polarisation matrix allows both η and γ to be determined.
- The effects of electric and magnetic fields on the domain population can be studied.
- When $\eta \neq 0$ the absolute directions of rotation of the neutron spins determine the magnetic configuration of the more populous domain.
- For these experiments the sample must be removed from the cryopad, warmed above its Néel temperature, then cooled through the Néel transition under the chosen conditions of electric and magnetic field.
- For Cr_2O_3 the symmetry of the magnetic structure suggests the fields should be applied parallel to the trigonal axis.
- Cooling with both electric and magnetic fields applied was needed to induce a reliably high domain ratio.

Stabilising domains in Cr_2O_3. Which field is "UP"?

Stabilising domains in Cr_2O_3. Which field is "UP"?

Introduction: The Blume Maleev Equations
First Experiments
Cryopad I
First steps in SNP
Cryopad II
Summary

- The Cr^{3+} in Cr_2O_3 ions are octahedrally coordinated by oxygen. with pairs of octahedra, sharing a common face.

Stabilising domains in Cr_2O_3. Which field is "UP"?

- The Cr^{3+} in Cr_2O_3 ions are octahedrally coordinated by oxygen. with pairs of octahedra, sharing a common face.
- The double octahedra are linked by sharing free vertices.

Stabilising domains in Cr_2O_3. Which field is "UP"?

Introduction: The Blume Maleev Equations
First Experiments
Cryopad I
First steps in SNP
Cryopad II
Summary

- The Cr^{3+} in Cr_2O_3 ions are octahedrally coordinated by oxygen. with pairs of octahedra, sharing a common face.
- The double octahedra are linked by sharing free vertices.
- Electric and magnetic fields, applied parallel to one another and to the c-axis while cooling through the Néel transition, stabilise the domain in which the moments point towards the shared face.

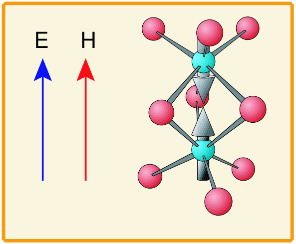

Cryopad II

The precision obtainable with CYOPAD I and its flexibility was limited by:

- The small diameter of the ϕ coils

Cryopad II

The precision obtainable with CYOPAD I and its flexibility was limited by:

- The small diameter of the ϕ coils
- Mutual inductance of the ϕ coils which varies with 2θ.

Cryopad II

The precision obtainable with CYOPAD I and its flexibility was limited by:

- The small diameter of the ϕ coils
- Mutual inductance of the ϕ coils which varies with 2θ.
- Interaction between the nutator fields at high 2θ.

Cryopad II

The precision obtainable with CYOPAD I and its flexibility was limited by:

- The small diameter of the ϕ coils
- Mutual inductance of the ϕ coils which varies with 2θ.
- Interaction between the nutator fields at high 2θ.
- Samples can't be cooled in magnetic fields in situ

Cryopad II

The precision obtainable with CYOPAD I and its flexibility was limited by:

- The small diameter of the ϕ coils
- Mutual inductance of the ϕ coils which varies with 2θ.
- Interaction between the nutator fields at high 2θ.
- Samples can't be cooled in magnetic fields in situ

The cryostat containing two cylindrical Meissner shields is in the form of a hollow cylinder.

The sample and its independent sample environment can be placed inside.

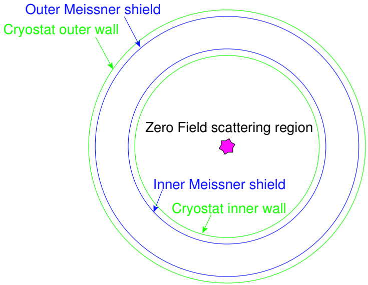

Cryopad II

The precision obtainable with CYOPAD I and its flexibility was limited by:

- The small diameter of the ϕ coils
- Mutual inductance of the ϕ coils which varies with 2θ.
- Interaction between the nutator fields at high 2θ.
- Samples can't be cooled in magnetic fields in situ

The cryostat containing two cylindrical Meissner shields is in the form of a hollow cylinder.

The sample and its independent sample environment can be placed inside.

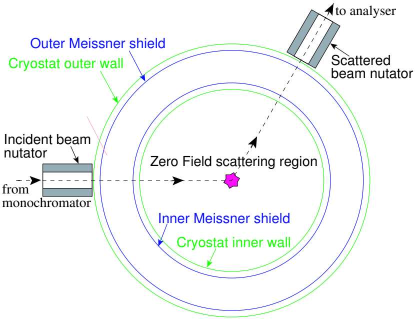

Cryopad II

The precision obtainable with CYOPAD I and its flexibility was limited by:

- The small diameter of the ϕ coils
- Mutual inductance of the ϕ coils which varies with 2θ.
- Interaction between the nutator fields at high 2θ.
- Samples can't be cooled in magnetic fields in situ

The cryostat containing two cylindrical Meissner shields is in the form of a hollow cylinder.

The sample and its independent sample environment can be placed inside.

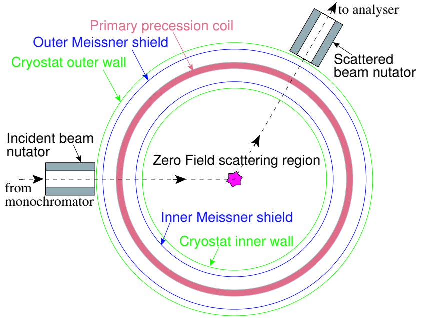

The precision obtainable with CYOPAD I and its flexibility was limited by:

- The small diameter of the ϕ coils
- Mutual inductance of the ϕ coils which varies with 2θ.
- Interaction between the nutator fields at high 2θ.
- Samples can't be cooled in magnetic fields in situ

The cryostat containing two cylindrical Meissner shields is in the form of a hollow cylinder.

The sample and its independent sample environment can be placed inside.

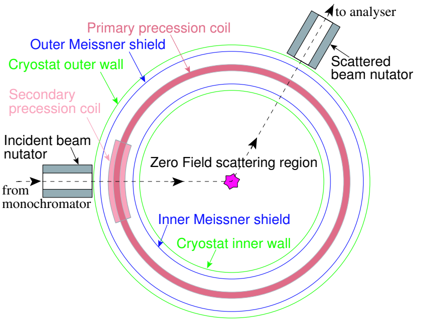

Transition metal orthophosphates: CRYOPAD II on IN20

The transition metal orthophosphates $LiTPO_4$ (T=Mn,Co,Ni) provide an interesting family of magnetoelectric compounds.

Transition metal orthophosphates: CRYOPAD II on IN20

The transition metal orthophosphates $LiTPO_4$ (T=Mn,Co,Ni) provide an interesting family of magnetoelectric compounds.

- All three have the same crystal structure, but order antiferromagnetically between 50 and 20 K with moments oriented parallel to different crystal axes.

Transition metal orthophosphates: CRYOPAD II on IN20

The transition metal orthophosphates $LiTPO_4$ (T=Mn,Co,Ni) provide an interesting family of magnetoelectric compounds.

- All three have the same crystal structure, but order antiferromagnetically between 50 and 20 K with moments oriented parallel to different crystal axes.
- This leads to different non-zero magnetoelectric coefficients.

Transition metal orthophosphates: CRYOPAD II on IN20

Introduction: The Blume Maleev Equations
First Experiments
Cryopad I
First steps in SNP
Cryopad II
Summary

The transition metal orthophosphates $LiTPO_4$ (T=Mn,Co,Ni) provide an interesting family of magnetoelectric compounds.

- All three have the same crystal structure, but order antiferromagnetically between 50 and 20 K with moments oriented parallel to different crystal axes.
- This leads to different non-zero magnetoelectric coefficients.
- For $LiCoPO_4$ α_{xy} and α_{yx} are non-zero.

Transition metal orthophosphates: CRYOPAD II on IN20

The transition metal orthophosphates $LiTPO_4$ (T=Mn,Co,Ni) provide an interesting family of magnetoelectric compounds.

- All three have the same crystal structure, but order antiferromagnetically between 50 and 20 K with moments oriented parallel to different crystal axes.
- This leads to different non-zero magnetoelectric coefficients.
- For $LiCoPO_4$ α_{xy} and α_{yx} are non-zero.
- Crossed electric and magnetic fields are needed to stabilise a particular 180° domain.

The transition metal orthophosphates $LiTPO_4$ (T=Mn,Co,Ni) provide an interesting family of magnetoelectric compounds.

- All three have the same crystal structure, but order antiferromagnetically between 50 and 20 K with moments oriented parallel to different crystal axes.
- This leads to different non-zero magnetoelectric coefficients.
- For $LiCoPO_4$ α_{xy} and α_{yx} are non-zero.
- Crossed electric and magnetic fields are needed to stabilise a particular 180° domain.

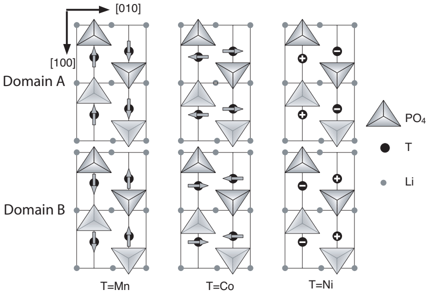

Transition metal orthophosphates: CRYOPAD II on IN20

The transition metal orthophosphates $LiTPO_4$ (T=Mn,Co,Ni) provide an interesting family of magnetoelectric compounds.

- All three have the same crystal structure, but order antiferromagnetically between 50 and 20 K with moments oriented parallel to different crystal axes.
- This leads to different non-zero magnetoelectric coefficients.
- For $LiCoPO_4$ α_{xy} and α_{yx} are non-zero.
- Crossed electric and magnetic fields are needed to stabilise a particular 180° domain.

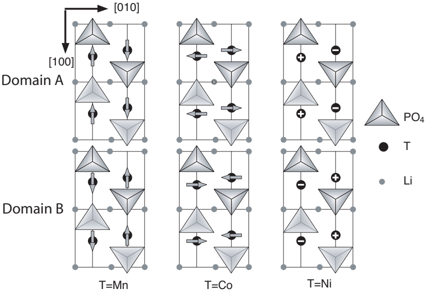

For $LiCoPO_4$

E	**H**	α	Dom.
$[\bar{1}00]$	$[0\bar{1}0]$	α_{xy}	A
$[100]$	$[0\bar{1}0]$	$-\alpha_{xy}$	B
$[010]$	$[\bar{1}00]$	$-\alpha_{yx}$	A
$[0\bar{1}0]$	$[\bar{1}00]$	α_{yx}	B

P.J. Brown, J.B. Forsyth and F. Tasset, *Solid State Sciences* **7** 682-689 (2005)

CRYOPAD on D3 with ^{3}He analyser

- IN20 is not really optimal for studying small crystals.

CRYOPAD on D3 with ^{3}He analyser

- IN20 is not really optimal for studying small crystals.
- Long scattering paths make the crystal orientation critical.

CRYOPAD on D3 with ^{3}He analyser

- IN20 is not really optimal for studying small crystals.
- Long scattering paths make the crystal orientation critical.
- Available wavelengths limit the accessible $\sin\theta/\lambda$ range.

CRYOPAD on D3 with ^{3}He analyser

- IN20 is not really optimal for studying small crystals.
- Long scattering paths make the crystal orientation critical.
- Available wavelengths limit the accessible $\sin\theta/\lambda$ range.
- The development of a ^{3}He polarising filter by Francis and collaborators made it possible to use CRYOPAD with the polarised neutron diffractometer D3 installed on the ILL hot source.

CRYOPAD on D3 with ^{3}He analyser

- IN20 is not really optimal for studying small crystals.
- Long scattering paths make the crystal orientation critical.
- Available wavelengths limit the accessible $\sin\theta/\lambda$ range.
- The development of a ^{3}He polarising filter by Francis and collaborators made it possible to use CRYOPAD with the polarised neutron diffractometer D3 installed on the ILL hot source.

D3 with Cryopad and Decpol

Antiferromagnetic form factors.

If a nearly single domain state can be stabilised in an a magnetoelectric crystal the ratio γ of magnetic to nuclear scattering can be determined rather precisely from experimentally determined polarisation matrices.

Antiferromagnetic form factors.

If a nearly single domain state can be stabilised in an a magnetoelectric crystal the ratio γ of magnetic to nuclear scattering can be determined rather precisely from experimentally determined polarisation matrices.

- Applies to antiferromagnetic structures for which the cross-section is not polarisation dependent.

Antiferromagnetic form factors.

If a nearly single domain state can be stabilised in an a magnetoelectric crystal the ratio γ of magnetic to nuclear scattering can be determined rather precisely from experimentally determined polarisation matrices.

- Applies to antiferromagnetic structures for which the cross-section is not polarisation dependent.
- The standard *flipping ratio* method cannot be used.

Antiferromagnetic form factors.

If a nearly single domain state can be stabilised in an a magnetoelectric crystal the ratio γ of magnetic to nuclear scattering can be determined rather precisely from experimentally determined polarisation matrices.

- Applies to antiferromagnetic structures for which the cross-section is not polarisation dependent.
- The standard *flipping ratio* method cannot be used.
- The polarisation is the ratio between two measurements made at constant cross-section, so extinction is not important.

Antiferromagnetic form factors.

If a nearly single domain state can be stabilised in an a magnetoelectric crystal the ratio γ of magnetic to nuclear scattering can be determined rather precisely from experimentally determined polarisation matrices.

- Applies to antiferromagnetic structures for which the cross-section is not polarisation dependent.
- The standard *flipping ratio* method cannot be used.
- The polarisation is the ratio between two measurements made at constant cross-section, so extinction is not important.

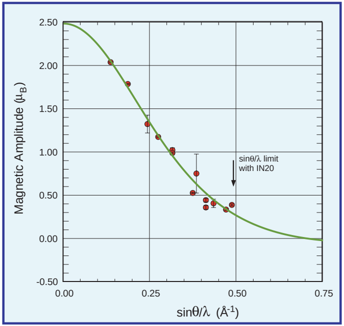

Antiferromagnetic form factors.

If a nearly single domain state can be stabilised in an a magnetoelectric crystal the ratio γ of magnetic to nuclear scattering can be determined rather precisely from experimentally determined polarisation matrices.

- Applies to antiferromagnetic structures for which the cross-section is not polarisation dependent.
- The standard *flipping ratio* method cannot be used.
- The polarisation is the ratio between two measurements made at constant cross-section, so extinction is not important.

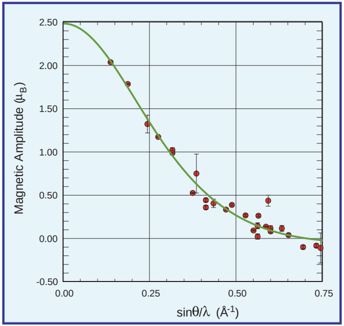

P.J. Brown, J.B. Forsyth and F. Tasset, *Physica B* **267-268** 215-220 (1999)

The magnetisation distribution in Cr_2O_3

The data can be used to make a maximum entropy reconstruction of the antiferromagnetic magnetisation distribution projected down [010].

The magnetisation distribution in Cr_2O_3

The data can be used to make a maximum entropy reconstruction of the antiferromagnetic magnetisation distribution projected down [010].

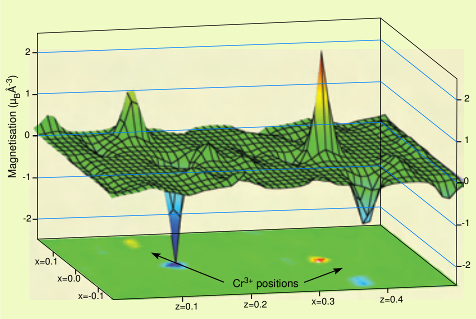

The coefficients of the reconstruction are differences between the observed structure factors and those calculated for an antiferromagnetic arrangement of Cr^{3+} ions with t_{2g} symmetry in the Cr_2O_3 structure

The magnetisation distribution in Cr_2O_3

The data can be used to make a maximum entropy reconstruction of the antiferromagnetic magnetisation distribution projected down [010].

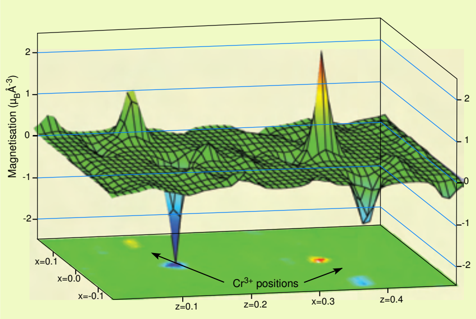

The coefficients of the reconstruction are differences between the observed structure factors and those calculated for an antiferromagnetic arrangement of Cr^{3+} ions with t_{2g} symmetry in the Cr_2O_3 structure

The difference density has a a gradient of magnetisation at the Cr^{3+} positions.

This may be the signature of the ME property.

P.J. Brown, J.B. Forsyth, E Lelièvre-Berna and F. Tasset,*J. Phys.: Condens Matter* **14** 1957-1966 (2002)

SNP: The dream realised?

- The spherical polarisation analysis technique has been in constant evolution over a period of more than 20 years.

SNP: The dream realised?

- The spherical polarisation analysis technique has been in constant evolution over a period of more than 20 years.
- The technical advances have been in large part due to Francis's dedication to the project and his insistence on excellence in its realisation.

SNP: The dream realised?

- The spherical polarisation analysis technique has been in constant evolution over a period of more than 20 years.
- The technical advances have been in large part due to Francis's dedication to the project and his insistence on excellence in its realisation.
- One should not forget the contribution made by Serge Pujol

SNP: The dream realised?

- The spherical polarisation analysis technique has been in constant evolution over a period of more than 20 years.
- The technical advances have been in large part due to Francis's dedication to the project and his insistence on excellence in its realisation.
- One should not forget the contribution made by Serge Pujol
- So! Is the dream now realised?

SNP: The dream realised?

- The spherical polarisation analysis technique has been in constant evolution over a period of more than 20 years.
- The technical advances have been in large part due to Francis's dedication to the project and his insistence on excellence in its realisation.
- One should not forget the contribution made by Serge Pujol
- So! Is the dream now realised? NEARLY

SNP: The dream realised?

- The spherical polarisation analysis technique has been in constant evolution over a period of more than 20 years.
- The technical advances have been in large part due to Francis's dedication to the project and his insistence on excellence in its realisation.
- One should not forget the contribution made by Serge Pujol
- So! Is the dream now realised? NEARLY
- We are only slowly learning how best to use SNP, to which problems it is particularly relevant and how to interpret the results.

SNP: The dream

NOT **THE END!**